Calculated OH-Stretching Vibrational Transitions in the Water−Nitrogen and Water−Oxygen Complexes

Henrik G. Kjaergaard,*,† Geoffrey R. Low, Timothy W. Robinson, and Daryl L. Howard

Department of Chemistry, University of Otago, P. O. Box 56, Dunedin, New Zealand

Received: February 26, 2002; In Final Form: June 18, 2002

We have calculated the fundamental and overtone OH-stretching vibrational band intensities of the water−nitrogen ($H_2O{\cdot}N_2$) and water−oxygen ($H_2O{\cdot}O_2$) complexes. The calculations use the harmonically coupled anharmonic oscillator local mode model with local mode parameters obtained from scaled ab initio calculations and ab initio calculated dipole moment functions. The $H_2O{\cdot}N_2$ and $H_2O{\cdot}O_2$ complexes are weakly bound and the individual molecular units are only slightly perturbed by complexation, unlike what is found for the water dimer ($H_2O{\cdot}H_2O$) and the water−nitric acid complex ($H_2O{\cdot}HNO_3$). The fundamental OH-stretching intensity in $H_2O{\cdot}N_2$ is enhanced and the first overtone intensity weakened compared to H_2O as an effect of the hydrogen bonding. In $H_2O{\cdot}O_2$ the OH-stretching intensities are comparable to those of H_2O. On a per water unit basis, the calculated OH-stretching intensities of the higher overtones of $H_2O{\cdot}N_2$ and $H_2O{\cdot}O_2$ are similar to those of $H_2O{\cdot}H_2O$. The possible effect of $H_2O{\cdot}N_2$ and $H_2O{\cdot}O_2$ on the atmospheric absorption of solar radiation is discussed.

Introduction

The discrepancy between observed and modeled atmospheric absorption of solar radiation is a long-standing problem in atmospheric science.[1−4] Water is the principal absorber of solar radiation, and in the near-infrared and visible regions its absorption spectrum is dominated by OH-stretching overtone transitions. Weakly bound van der Waals complexes, especially those containing water, have been suggested as possible contributors to the excess or anomalous solar absorption.[5−9] In the atmosphere, where the gas is not strongly pressurized, the principal complexes formed are the 1:1 complexes.[9] Previously, we have investigated the OH-stretching overtone spectra of the water dimer[10] ($H_2O{\cdot}H_2O$), and in the present article we investigate the water−nitrogen ($H_2O{\cdot}N_2$) and water−oxygen ($H_2O{\cdot}O_2$) complexes.

The large-amplitude motion associated with OH-stretching vibrations can be described in terms of local modes and the harmonically coupled anharmonic oscillator (HCAO) local mode model.[11−13] Overtone intensities have been successfully predicted with the HCAO local mode model and ab initio calculated dipole moment functions at modest ab initio levels.[14−17] Calculations on the water monomer have shown that the simple HCAO local mode model is an adequate vibrational model compared to a full variational calculation,[18] and the results obtained are in good agreement with the experimental intensities of the HITRAN database.[19] Basis sets of triple-ζ quality including diffuse and polarization functions were required to obtain accurate absolute intensities for the water molecule.[20] We have previously observed for monomeric species that the inclusion of electron correlation is important for the accurate prediction of fundamental intensities, but less so for the overtone intensities.[21]

We have recently suggested a method that allows the calculation of OH-stretching overtone spectra without the need of input from experimental spectra.[10] The method is based on suggestions by Sowa et al.[22] to obtain the local mode parameters from ab initio calculated potential energy curves.[10] We have used this method to calculate the OH-stretching transitions for the water dimer and trimer[10] and for the water−nitric acid ($H_2O{\cdot}HNO_3$) complex.[23] These calculated overtone spectra indicate spectral regions that are favorable for experimental investigations of these complexes.

Infrared (IR) spectra of $H_2O{\cdot}N_2$ trapped in cold Ar matrixes have been recorded,[24,25] and the vapor phase structure has been determined by microwave studies.[26] No vibrational spectra of $H_2O{\cdot}O_2$ have been recorded, nor has the experimental structure been determined. However, recent neutralization−reionization mass spectroscopy studies have found evidence for the presence of both $H_2O{\cdot}O_2$ and the charge-transfer complex $H_2O^+{\cdot}O_2^-$, with the neutral species having a lifetime exceeding 0.5 μs.[27]

There have been a number of theoretical investigations regarding the structure and IR spectra of the $H_2O{\cdot}N_2$ and $H_2O{\cdot}O_2$ complexes.[25,28−31] The theoretical predictions for $H_2O{\cdot}N_2$ compare reasonably well with the experimental matrix isolation IR spectra[24,25] and with the microwave determined structure.[26] Theoretical studies of $H_2O{\cdot}O_2$ have focused predominantly on its role in the photonucleation of water vapor in the presence of oxygen, a first step in cloud formation. It is suggested that UV radiation incident on the $H_2O{\cdot}O_2$ complex stimulates an electron-transfer process creating a charge-transfer product $H_2O^+{\cdot}O_2^-$ that is thought to function as an aggregation point for nearby polar water molecules.[32,33]

We report HCAO calculated fundamental and overtone OH-stretching band positions and intensities for $H_2O{\cdot}N_2$ and $H_2O{\cdot}O_2$ and compare our results with calculations for H_2O, $H_2O{\cdot}H_2O$, and $H_2O{\cdot}HNO_3$. We compare our results for $H_2O{\cdot}N_2$ with the available experimental IR data[24,25] and for $H_2O{\cdot}H_2O$ with the molecular beam IR data[34,35] and the recent IR and near-IR (NIR) matrix isolation data.[36,37]

* Corresponding author. Telephone: 64-3-479-5378. Fax: 64-3-479-7906. E-mail: henrik@alkali.otago.ac.nz.

† On sabbatical at Cooperative Institute for Research in Environmental Sciences (CIRES), University of Colorado, Boulder, CO 80309-0216.

10.1021/jp020542y CCC: $22.00
Published on Web 08/30/2002

In general, fundamental vibrations of OH bonds involved in hydrogen bonding undergo frequency red shifts and intensity enhancement.[38] Studies of liquid-phase spectra observed a significant weakening of the first overtone OH-stretching transitions upon hydrogen bonding.[39] This result has recently been corroborated by matrix isolation studies on $H_2O{\cdot}H_2O$[36,37] and is in good agreement with our theoretical prediction.[10] In this article, we explain this intensity pattern in terms of transition dipole matrix elements and dipole derivatives.

The contribution to atmospheric absorption of solar radiation from a complex depends on the absorption spectra in the relevant spectral regions and the abundance of the complex. Electronic transitions in the weakly bound $O_2{\cdot}O_2$ complex have been observed in the atmosphere,[40] and together with $O_2{\cdot}N_2$ their contribution to the absorption of solar radiation is estimated at about 1 W/m^2.[40,41] On the basis of our previously calculated OH-stretching spectra of $H_2O{\cdot}H_2O$,[10] its absorption of solar radiation has been estimated at a global average of about 0.5 W/m^2.[42] The abundances of $H_2O{\cdot}N_2$ and $H_2O{\cdot}O_2$ have been estimated to be an order of magnitude larger than that of $H_2O{\cdot}H_2O$.[8,28,43] Thus $H_2O{\cdot}N_2$ and $H_2O{\cdot}O_2$ could potentially contribute significantly to atmospheric absorption of solar radiation, and the extent depends on the absorption spectra of these complexes.

Theory and Calculations

The dimensionless oscillator strength f of a transition from the ground vibrational state "g" to an excited vibrational state "e" is given by[16,44]

$$f_{eg} = 4.702 \times 10^{-7}[\text{cm D}^{-2}]\tilde{\nu}_{eg}|\vec{\mu}_{eg}|^2 \qquad (1)$$

where $\tilde{\nu}_{eg}$ is the frequency of the transition in wavenumbers and $\vec{\mu}_{eg} = \langle e|\vec{\mu}|g\rangle$ is the transition dipole moment matrix element in Debye (D). Thus both the vibrational wave functions and the dipole moment function are required to calculate vibrational band intensities and simulate overtone spectra.

Vibrational Model. We use the HCAO local mode model to obtain the vibrational energies and wave functions. The water units of the $H_2O{\cdot}N_2$ and $H_2O{\cdot}O_2$ complexes are treated as two coupled anharmonic OH-stretching oscillators. The water unit in the calculated lowest energy structures of $H_2O{\cdot}N_2$ and $H_2O{\cdot}O_2$ is asymmetric with two nonequivalent OH bonds. The asymmetric water units are treated similarly to the asymmetric CH_2 groups of cyclohexane, as described in detail elsewhere.[15] We label the OH oscillators OH_b for the hydrogen closest to the O_2 or N_2 unit and OH_f for the hydrogen farthest away from the O_2 or N_2 unit, similar to the notation we used for the hydrogen donor water unit in $H_2O{\cdot}H_2O$.[10]

Briefly, the local mode model zero-order Hamiltonian for the asymmetric H_bOH_f group is written[15]

$$(H - E_{|00\rangle})/hc = \upsilon_b\tilde{\omega}_b - (\upsilon_b^2 + \upsilon_b)\tilde{\omega}_b x_b + \upsilon_f\tilde{\omega}_f - (\upsilon_f^2 + \upsilon_f)\tilde{\omega}_f x_f \qquad (2)$$

with each of the two OH-stretching potentials described by a Morse potential. $E_{|00\rangle}$ is the energy of the vibrational ground state, υ_b and υ_f are the vibrational quantum numbers, and $\tilde{\omega}$ and $\tilde{\omega}x$ are the frequencies and anharmonicities of the local mode oscillators, respectively. The zero-order basis states for the Hamiltonian are product functions of two different Morse oscillator wave functions, and can be written as $|\upsilon_b\rangle_b|\upsilon_f\rangle_f$. The total number of OH-stretching quanta is given by $\upsilon_b + \upsilon_f = \upsilon$, and states with the same υ belong to a vibrational manifold.

The coupling between the two nonequivalent OH oscillators in the H_bOH_f unit is limited to the harmonic coupling within a given manifold and gives rise to the perturbation[15]

$$H'/hc = -\gamma'_{bf}(a_b a_f^\dagger + a_b^\dagger a_f) \qquad (3)$$

where $a^\dagger$ and a are the step-up and step-down operators known from harmonic oscillators,[45] and the effective intramanifold coupling coefficient[15]

$$\gamma'_{bf} = (\gamma_{bf} - \phi_{bf})\sqrt{\tilde{\omega}_b\tilde{\omega}_f} = \left(-\frac{\cos\theta}{2}\left(1 + \frac{m_O}{m_H}\right)^{-1} - \frac{1}{2}\frac{F_{bf}}{\sqrt{F_{bb}F_{ff}}}\right)\sqrt{\tilde{\omega}_b\tilde{\omega}_f} \qquad (4)$$

includes both kinetic and potential energy coupling terms. The kinetic energy coupling term γ_{bf} is dependent on the Wilson **G**-matrix elements and can therefore be determined from the ab initio calculated optimized geometry. The potential energy coupling term ϕ_{bf} can be determined from the ab initio calculated force constants. In eq 4, θ is the H_bOH_f angle, m_O and m_H are the atomic masses, F_{bb} and F_{ff} are the diagonal force constants, and F_{bf} is the off-diagonal force constant.

Diagonalization of the Hamiltonian, eqs 2 and 3, gives the eigenenergies and vibrational wave functions. Due to the small effect of N_2 (O_2) on the water unit, the two OH oscillators in $H_2O{\cdot}N_2$ ($H_2O{\cdot}O_2$) are very similar, in contrast to what we have observed for the hydrogen donor water unit in $H_2O{\cdot}H_2O$.[10]

Calculation of Local Mode Parameters. The Morse oscillator frequency $\tilde{\omega}$ and anharmonicity $\tilde{\omega}x$ can be written in terms of the Morse oscillator parameters D and a and the reduced mass of the OH bond. Expansion of the Morse potential shows that the parameters D and a can be expressed by the second- and third-order force constants F_{ii} and F_{iii}. The following expressions are obtained for the local mode frequency and anharmonicity in wavenumbers:[10,22]

$$\tilde{\omega} = \frac{\omega}{2\pi c} = \frac{(F_{ii}G_{ii})^{1/2}}{2\pi c} \qquad (5)$$

$$\tilde{\omega}x = \frac{\omega x}{2\pi c} = \frac{hG_{ii}}{72\pi^2 c}\left(\frac{F_{iii}}{F_{ii}}\right)^2 \qquad (6)$$

where G_{ii} is the inverse of the reduced mass of the OH bond.

We calculate F_{ii} and F_{iii} by standard numerical procedures from a one-dimensional grid of ab initio calculated potential energies. The grid is calculated by displacing the internal displacement coordinate q by ± 0.2 Å from the equilibrium position in steps of 0.05 Å. We have found that a nine-point grid with a step size of 0.05 Å steps gives good convergence of the potential energy derivatives (force constants).[10,15]

We have scaled the ab initio calculated local mode parameters similarly to the commonly used scaling of ab initio calculated harmonic frequencies.[10,46] The scaling of harmonic frequencies is done in part to compensate for neglect of anharmonicity in the potentials and in part to compensate for limitations in the accuracy of the ab initio method employed. We scale our local mode parameters to compensate for inaccuracy in the ab initio method and to a much lesser extent deficiencies of the Morse potential. Briefly, we calculate the ab initio local mode parameters for H_2O for which high-quality experimental values for $\tilde{\omega}$ and $\tilde{\omega}x$ are known. The ratio of calculated to experimental local mode parameters for H_2O determines scaling factors suitable for hydrated complexes.

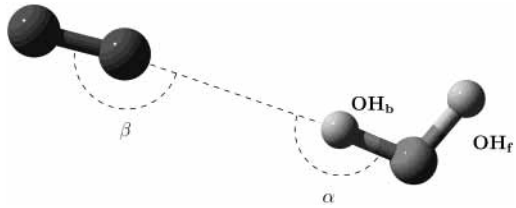

Figure 1. QCISD/6-311++G(2d,2p) optimized geometry of the $H_2O\cdot N_2$ complex. The structure has C_s symmetry. Bond lengths: OH_b = 0.957 Å, OH_f = 0.956 Å, and N_2 = 1.098 Å. Angles: HOH = 104.7°, α = 172.8°, and β = 176.1°.

Dipole Moment Function. The dipole moment function is approximated by a series expansion in the internal OH displacement coordinates about the equilibrium geometry. For the H_bOH_f group we have[15]

$$\vec{\mu}(q_b,q_f) = \sum_{i,j} \vec{\mu}_{ij} q_b^{\,i} q_f^{\,j} \tag{7}$$

where the coefficients $\vec{\mu}_{ij}$ are given by

$$\vec{\mu}_{ij} = \frac{1}{i!j!} \frac{\partial^{i+j}\vec{\mu}}{\partial q_b^{\,i}\, \partial q_f^{\,j}} \tag{8}$$

The summation in eq 7 is limited to fifth-order diagonal and third-order mixed terms, based on previous work.[10,15,47] The coefficients $\vec{\mu}_{ij}$ are calculated by standard numerical techniques from a two-dimensional dipole moment grid, $\vec{\mu}(q_b,q_f)$. The grid is calculated by displacing the internal displacement coordinates q_b and q_f of the two OH oscillators by ±0.2 Å from equilibrium in steps of 0.05 Å. The grid size and step size chosen provide good convergence of the dipole moment derivatives.[10,15,47]

The geometry optimizations and grid point calculations for the specific ab initio methods were all performed with the use of Gaussian94.[48] The dipole moment at each point was calculated using the density matrix for the current method, to provide dipole moments that are the correct analytical derivatives of the energy. We have limited the present study to the self-consistent-field Hartree−Fock (HF), the correlated quadratic configuration interaction including singles and doubles (QCISD), and Becke's three-parameter hybrid method with the Lee−Yang−Parr correlation functional (B3LYP) theories with the 6-31G(d), 6-311+G(d,p), and 6-311++G(2d,2p) basis sets. The ground state of $H_2O\cdot O_2$ is a triplet, and unrestricted wave functions have been used. All geometries were optimized with "tight" convergence limits and confirmed as minima by frequency calculations resulting in zero imaginary frequencies.

Results and Discussion

The potential energy surfaces for $H_2O\cdot N_2$ and $H_2O\cdot O_2$ are known to be flat, and a number of possible structures have been suggested.[25,28−30,33,49] The QCISD/6-311++G(2d,2p) optimized structures for $H_2O\cdot N_2$ and $H_2O\cdot O_2$ are shown in Figures 1 and 2 (hereafter referred to as structures **1** and **2**), respectively. The figures illustrate the labeling used, and selected optimized parameters are given in the captions.

Structure **1** is the lowest energy configuration for $H_2O\cdot N_2$ at all levels of theory, in agreement with recent theoretical studies.[25,28,30] The QCISD/6-311++G(2d,2p) calculated value of the *B* rotational constant for $H_2O\cdot N_2$ is 2.92 GHz, in excellent agreement with the experimentally determined value of 2.91 GHz.[26] The calculated intermolecular (O···N) distance is 3.35 Å, which compares well with the experimental value of 3.37 Å.[26] The angle α is calculated to be 173° compared to the

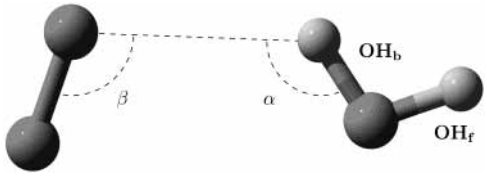

Figure 2. QCISD/6-311++G(2d,2p) optimized geometry of the $H_2O\cdot O_2$ complex. The structure has C_s symmetry. Bond lengths: OH_b = 0.957 Å, OH_f = 0.956 Å, and O_2 = 1.209 Å. Angles: HOH = 104.7°, α = 125.8°, and β = 108.9°.

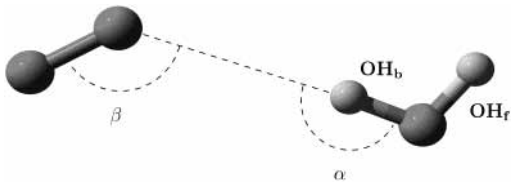

Figure 3. HF/6-311++G(2d,2p) optimized geometry of the $H_2O\cdot O_2$ complex. The structure has C_s symmetry. Bond lengths: OH_b = 0.940 Å, OH_f = 0.940 Å, and O_2 = 1.162 Å. Angles: HOH = 106.3°, α = 175.4°, and β = 132.6°.

experimental value of 169°,[26] which makes the conformation of $OH_b\cdots N$ bond close to linear, as is commonly observed for hydrogen bonds.[50]

Previous theoretical studies on $H_2O\cdot O_2$ have found a number of possible low-energy structures differing only slightly in their relative energies.[28,31−33,51] The flatness of the potential surface is in agreement with the observation that the optimized $H_2O\cdot O_2$ configuration is dependent on the basis set and level of theory used. Our highest quality geometry optimizations with the QCISD/6-311+G(d,p) and QCISD/6-311++G(2d,2p) methods give structure **2** as the global minimum energy configuration with zero imaginary frequencies. All HF and B3LYP calculations with the three basis sets used give the configuration shown in Figure 3 (structure **3**) as the global minimum, except for the HF/6-311+G(d,p) calculation which gives structure **2**. The QCISD/6-31G(d) method yields both structures **2** and **3** as minima with no imaginary frequencies, with structure **3** slightly lower in energy by 0.3 kcal/mol. To our knowledge, structure **2** has not been reported as the energy minimum for $H_2O\cdot O_2$ in previous studies.

The majority of previous theoretical studies on $H_2O\cdot O_2$ have concentrated only on C_{2v} ground state geometries, to maximize the possibility of converging to the charge-transfer electronically excited state.[32,33] A recent study with the MP2(full)/6-311++G(2d,2p) method did consider C_s geometries and found a linear "hydrogen bonded" configuration as the minimum.[28] We have found, however, that the MP2(full)/6-311++G(2d,2p) calculated energy for structure **2** is about 0.1 kcal/mol lower than that reported for the linear hydrogen bonded configuration. The main difference between the optimized $H_2O\cdot O_2$ structures **2** and **3** is the significantly smaller value of α for structure **2**. The $H_2O\cdot O_2$ structures **2** and **3** have significantly different rotational constants, and microwave spectroscopy should be able to resolve this structural uncertainty.

In agreement with previous theoretical studies, we find that the formation of $H_2O\cdot N_2$ and $H_2O\cdot O_2$ has a small effect on the structural parameters of the monomeric units.[25,28,29] This is in contrast to $H_2O\cdot H_2O$, where significant changes in OH bond lengths are observed for the hydrogen donor water unit. The calculated permanent dipole moments of the QCISD/6-311++G(2d,2p) optimized structures are 2.08 D for $H_2O\cdot N_2$ and 1.80 D for $H_2O\cdot O_2$, which are close to the calculated value of 1.96 D for H_2O. In comparison, the calculated dipole moment

TABLE 1: Local Mode Parameters (in cm^{-1}) for $H_2O \cdot N_2$, $H_2O \cdot O_2$, and the Hydrogen Donor Water Unit of $H_2O \cdot H_2O$[a]

	OH_b		OH_f		
	$\tilde{\omega}$	$\tilde{\omega}x$	$\tilde{\omega}$	$\tilde{\omega}x$	γ'_{bf}
$H_2O \cdot N_2$	3873	81.0	3872	82.2	47.2
$H_2O \cdot O_2$	3870	81.8	3869	82.1	48.3
$H_2O \cdot H_2O$	3782	85.5	3879	82.3	44.2

[a] Calculated with the QCISD/6-311++G(2d,2p) method and scaled with 0.9836 and 0.851 for $\tilde{\omega}$ and $\tilde{\omega}x$, respectively. The experimental local mode parameters for the water monomer are $\tilde{\omega} = 3869.9$ cm^{-1}, $\tilde{\omega}x = 82.06$ cm^{-1}, and $\gamma' = 49.44$ cm^{-1} from ref 18.

for $H_2O \cdot H_2O$ is 2.68 D, indicative of a much larger interaction between the monomeric units.

The calculated binding energies of $H_2O \cdot N_2$ and $H_2O \cdot O_2$ are small and significantly less than that of $H_2O \cdot H_2O$, and they increase from HF to B3LYP to QCISD theories. For the range of methods used, the calculated binding energy of $H_2O \cdot N_2$ is approximately twice as large as that calculated for $H_2O \cdot O_2$. The QCISD/6-311++G(2d,2p) calculated binding energy of $H_2O \cdot H_2O$ is 5.1 kcal/mol, in good agreement with the experimentally determined binding energies of 4.9 kcal/mol[52] and 5.4 kcal/mol.[53] We believe, therefore, that the QCISD/6-311++G(2d,2p) calculated binding energies of 1.29 and 0.72 kcal/mol for $H_2O \cdot N_2$ and $H_2O \cdot O_2$, respectively, are reasonable. Despite the much smaller binding energies, the existence of both $H_2O \cdot N_2$ and $H_2O \cdot O_2$ has been verified experimentally.[24-27]

Scaling Factors and Local Mode Parameters. Ideally the local mode parameters $\tilde{\omega}$, $\tilde{\omega}x$, and γ'_{bf} are determined from experiment; however, this is not possible for $H_2O \cdot N_2$ and $H_2O \cdot O_2$. We have recently shown that scaled local mode parameters were able to accurately reproduce the experimentally observed fundamental transition frequencies of $H_2O \cdot H_2O$.[10] The QCISD/6-311++G(2d,2p) calculated and scaled local mode parameters for $H_2O \cdot N_2$ and $H_2O \cdot O_2$ are given in Table 1, and are compared to those of the hydrogen donor water unit of $H_2O \cdot H_2O$. The OH_b oscillator in $H_2O \cdot H_2O$ is characterized by a significantly decreased value for the local mode frequency $\tilde{\omega}$ and an increased anharmonicity $\tilde{\omega}x$ compared to H_2O. Such significant shifts are not observed for the OH oscillators in $H_2O \cdot N_2$ and $H_2O \cdot O_2$, consistent with the small structural perturbations on complexation.

The calculated effective coupling parameters γ'_{bf} are also given in Table 1. The effective coupling parameter affects the distribution of intensity between states within a vibrational manifold. The values of γ'_{bf} for $H_2O \cdot N_2$ and $H_2O \cdot O_2$ are close to that for H_2O. The calculated γ'_{bf} value of 47.2 cm^{-1} for $H_2O \cdot N_2$ is consistent with the observed splitting of the two fundamental transitions of 89.4 cm^{-1} in the matrix isolation spectra.[25]

Fundamental Vibrations. We have calculated frequencies and intensities of the vibrational normal modes in $H_2O \cdot N_2$ and $H_2O \cdot O_2$ with the harmonic oscillator linear dipole moment approximation (HOLD) implemented in Gaussian94 and the frequencies and intensities of OH-stretching transitions with the HCAO local mode model with the use of nonlinear dipole moment functions. The HOLD calculated frequencies and intensities are given in Table 2. The experimentally determined fundamental frequencies and relative intensities of $H_2O \cdot N_2$ are given in Table 3.[25] The asymmetric stretching, symmetric stretching, and bending vibrations of the water unit are labeled ν_3, ν_1, and ν_2, and the N_2 (O_2) stretching vibration is labeled ν_4.[29] In the matrix isolation spectra of $H_2O \cdot N_2$ the frequencies of the four fundamental transitions are shifted by less than 5 cm^{-1} compared to those of the monomers,[24,25] as might be expected from the small changes in calculated geometry on formation of the complex. The observed shifts are similar to the shifts predicted in the HOLD calculations.

TABLE 2: Calculated Fundamental Vibrational Frequencies and Intensities with the HOLD Method for H_2O, $H_2O \cdot N_2$, and $H_2O \cdot O_2$[a]

	$H_2O \cdot N_2$		$H_2O \cdot O_2$		H_2O	
mode	$\tilde{\nu}$ (cm^{-1})	f	$\tilde{\nu}$ (cm^{-1})	f	$\tilde{\nu}$ (cm^{-1})	f
ν_3	3983	2.08×10^{-5}	3979	1.22×10^{-5}	3982	1.05×10^{-5}
ν_1	3884	0.47×10^{-5}	3877	0.09×10^{-5}	3878	0.13×10^{-5}
ν_2	1693	1.00×10^{-5}	1685	1.44×10^{-5}	1686	1.23×10^{-5}
ν_4	2388[b]	0.06×10^{-6}	1615[b]	0.02×10^{-5}		

[a] Harmonic oscillator linear dipole calculation within Gaussian94 with the QCISD/6-311++G(2d,2p) method. [b] For N_2 and O_2 the calculated frequencies are 2383 and 1621 cm^{-1}, respectively, both with zero intensity.

TABLE 3: Observed and Calculated Relative Intensities in $H_2O \cdot N_2$ and $H_2O \cdot O_2$[a]

	$H_2O \cdot N_2$				$H_2O \cdot O_2$	
mode	$\tilde{\nu}_{obs}$[b] (cm^{-1})	f_{obs}[b]	f_{calc}[c]	f_{calc}[d]	f_{calc}[c]	f_{calc}[d]
ν_3	3729.6	1.00	1.00	1.00	1.00	1.00
ν_1	3640.2	0.36	0.23	0.25	0.07	0.07
ν_2	1593	0.63	0.48		1.18	
ν_4	2329.3	0.02	0.003		0.02	

[a] The intensities are relative to the ν_3 band strength. [b] Taken from ref 25. [c] QCISD/6-311++G(2d,2p) calculation within Gaussian94 with the HOLD method. [d] QCISD/6-311++G(2d,2p) calculation with the HCAO method.

There have been no experimental IR spectra observed for the $H_2O \cdot O_2$ complex. We could not reproduce the large calculated shift of 46 cm^{-1} for the ν_4 transition reported in the previous ab initio study,[28] and compared to $H_2O \cdot N_2$ one would predict smaller frequency shifts for $H_2O \cdot O_2$ due to the lower binding energy and smaller geometric perturbations.

In $H_2O \cdot N_2$ and $H_2O \cdot O_2$ the OH_b and OH_f bonds are almost equivalent and significant mixing of states occurs in the fundamental and lower overtone regions. Thus it is meaningful to talk of symmetric ν_1 and asymmetric ν_3 vibrations similar to the vibrations in H_2O. This is in contrast to the hydrogen donor unit of $H_2O \cdot H_2O$, for which the OH_b and OH_f are significantly different and the state mixing is much less. In H_2O, $H_2O \cdot N_2$, and $H_2O \cdot O_2$ the intensity of the higher energy ν_3 band is larger than the intensity of the lower energy ν_1 band. However, in $H_2O \cdot H_2O$ the intensity of the lower energy OH_b-stretching band is the most intense band in the fundamental region.

The HOLD and HCAO calculations give relative fundamental OH-stretching transition intensities that are in good agreement with the experimental results[25] as seen in Table 3. Consistent with previous studies, we observe an increase in the calculated intensity of the ν_3 and ν_1 bands on formation of the complexes.[25,28,29] The increase is minor for $H_2O \cdot O_2$ and about a factor of 2 for $H_2O \cdot N_2$.

DFT Methods and Hydrogen-Bonded Vibrations. It is generally regarded that almost all of the widely used density functional methods fail to predict correctly the shift of OH-stretching transition frequencies occurring on hydrogen bond formation.[54] Theoretical studies that compare calculated to experimental fundamental OH-stretching frequency shifts generally employ a harmonic potential approximation, a scheme not well suited to OH-stretching vibrations, which are known to be highly anharmonic in nature. The HCAO calculated OH-

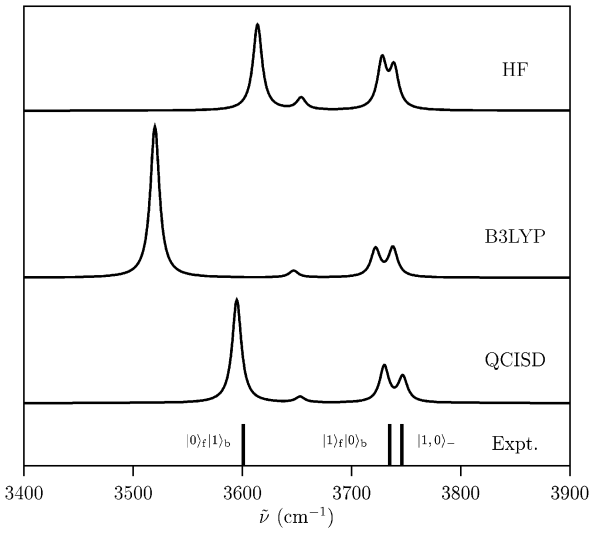

Figure 4. Simulated spectra of $H_2O{\cdot}H_2O$ in the $\Delta v_{OH} = 1$ region. The vibrational transitions were calculated with the HF, B3LYP, and QCISD levels of theory and the 6-311++G(2d,2p) basis set, and convoluted with Lorentzian functions with a fwhm of 10 cm^{-1}. Experimental peak positions are taken from refs 34 and 35 and are shown with arbitrary intensity.

stretching fundamental spectra of $H_2O{\cdot}H_2O$ with the HF, B3LYP, and QCISD methods and the three experimentally observed transitions are shown in Figure 4.[34,35] The B3LYP calculated frequency shift of the OH_b-stretching transition is overestimated by about 70 cm^{-1}. This result shows that the failure of the B3LYP method in predicting the OH_b-stretching frequency cannot be explained simply as an effect of anharmonicity, as anharmonicity is included in the HCAO local mode model, but rather must be due to inherent errors in the density functional method itself. Much better agreement is found for the HF and QCISD methods, where the HF calculation slightly underestimates and the QCISD calculation slightly overestimates the shift in OH_b-stretching frequency.

OH-Stretching Transitions. The HCAO calculated frequencies and intensities of the OH-stretching transitions in $H_2O{\cdot}N_2$ and $H_2O{\cdot}O_2$ are given in Tables 4 and 5, respectively. We present only the results obtained with the QCISD/6-311++G(2d,2p) method. The HCAO calculated OH-stretching fundamental frequencies for $H_2O{\cdot}N_2$ are about 25 cm^{-1} larger than those observed in the Ar matrix spectra.[25] However, it is known that matrix effects can shift vibrational frequencies. For $H_2O{\cdot}H_2O$, the HCAO calculated fundamental frequencies with the QCISD/6-311++G(2d,2p) method[10] are close to those of the molecular beam experiments,[34,35] whereas the transitions observed in the Ar matrix IR spectra[36] are red shifted by about 25 cm^{-1}.

The simulated OH-stretching vibrational spectra of $H_2O{\cdot}H_2O$, $H_2O{\cdot}N_2$, and $H_2O{\cdot}O_2$ in the $\Delta v_{OH} = 4$ region are shown in Figure 5. Each of the QCISD/6-311++G(2d,2p) calculated transitions has been convoluted with a Lorentzian line profile with a full width at half-maximum (fwhm) of 40 cm^{-1}, similar to the line widths observed in overtone spectra of small molecules.[16,17] For comparison we show a simulated H_2O spectrum, generated with the experimental frequencies and intensities from the HITRAN spectral database[19] convoluted with Gaussian line profiles with fwhm of 2 cm^{-1}. The H_2O spectrum has two vibrational transitions each with a P and R rotational branch. The OH-stretching bands of both $H_2O{\cdot}N_2$ and $H_2O{\cdot}O_2$ are not significantly shifted from the centers of the two H_2O vibrational bands. The experimental band shapes of the complexes are not expected to display rotational structure similar to that of H_2O, due to the larger sizes of the complexes and their shorter lifetimes.

TABLE 4: Calculated OH-Stretching Frequencies and Intensities for $H_2O{\cdot}N_2$[a]

state	$\tilde{\nu}$/cm^{-1}	f
$\|1\rangle_f\|0\rangle_b$	3 662	0.48×10^{-5}
$\|0\rangle_f\|1\rangle_b$	3 756	1.87×10^{-5}
$\|2\rangle_f\|0\rangle_b$	7 212	1.19×10^{-7}
$\|0\rangle_f\|2\rangle_b$	7 255	4.52×10^{-7}
$\|1\rangle_f\|1\rangle_b$	7 461	7.96×10^{-9}
$\|3\rangle_f\|0\rangle_b$	10 608	0.60×10^{-8}
$\|0\rangle_f\|3\rangle_b$	10 626	1.41×10^{-8}
$\|2\rangle_f\|1\rangle_b$	10 896	0.29×10^{-9}
$\|1\rangle_f\|2\rangle_b$	11 074	3.77×10^{-9}
$\|4\rangle_f\|0\rangle_b$	13 826	4.41×10^{-10}
$\|0\rangle_f\|4\rangle_b$	13 852	4.42×10^{-10}
$\|3\rangle_f\|1\rangle_b$	14 261	0.27×10^{-10}
$\|1\rangle_f\|3\rangle_b$	14 364	2.50×10^{-10}
$\|5\rangle_f\|0\rangle_b$	16 877	3.96×10^{-11}
$\|0\rangle_f\|5\rangle_b$	16 915	3.45×10^{-11}
$\|4\rangle_f\|1\rangle_b$	17 508	0.42×10^{-11}
$\|1\rangle_f\|4\rangle_b$	17 550	1.75×10^{-11}
$\|6\rangle_f\|0\rangle_b$	19 764	5.38×10^{-12}
$\|0\rangle_f\|6\rangle_b$	19 816	4.41×10^{-12}
$\|5\rangle_f\|1\rangle_b$	20 575	1.18×10^{-12}
$\|1\rangle_f\|5\rangle_b$	20 610	1.11×10^{-12}

[a] Calculated with the QCISD/6-311++G(2d,2p) method and local mode parameters from Table 1.

TABLE 5: Calculated OH-Stretching Frequencies and Intensities for $H_2O{\cdot}O_2$[a]

state	$\tilde{\nu}$/cm^{-1}	f
$\|1\rangle_f\|0\rangle_b$	3 657	0.07×10^{-5}
$\|0\rangle_f\|1\rangle_b$	3 754	0.94×10^{-5}
$\|2\rangle_f\|0\rangle_b$	7 203	0.94×10^{-7}
$\|0\rangle_f\|2\rangle_b$	7 247	6.27×10^{-7}
$\|1\rangle_f\|1\rangle_b$	7 456	2.02×10^{-9}
$\|3\rangle_f\|0\rangle_b$	10 598	0.15×10^{-8}
$\|0\rangle_f\|3\rangle_b$	10 609	2.51×10^{-8}
$\|2\rangle_f\|1\rangle_b$	10 883	0.22×10^{-9}
$\|1\rangle_f\|2\rangle_b$	11 065	4.14×10^{-9}
$\|4\rangle_f\|0\rangle_b$	13 817	3.15×10^{-10}
$\|0\rangle_f\|4\rangle_b$	13 823	5.56×10^{-10}
$\|3\rangle_f\|1\rangle_b$	14 243	0.25×10^{-10}
$\|1\rangle_f\|3\rangle_b$	14 349	2.73×10^{-10}
$\|5\rangle_f\|0\rangle_b$	16 867	3.52×10^{-11}
$\|0\rangle_f\|5\rangle_b$	16 875	3.99×10^{-11}
$\|4\rangle_f\|1\rangle_b$	17 486	0.22×10^{-11}
$\|1\rangle_f\|4\rangle_b$	17 525	2.15×10^{-11}
$\|6\rangle_f\|0\rangle_b$	19 753	4.91×10^{-12}
$\|0\rangle_f\|6\rangle_b$	19 763	5.31×10^{-12}
$\|5\rangle_f\|1\rangle_b$	20 559	0.49×10^{-12}
$\|1\rangle_f\|5\rangle_b$	20 569	2.06×10^{-12}

[a] Calculated with the QCISD/6-311++G(2d,2p) method and local mode parameters from Table 1.

In Figure 6 we show the ratio of total OH-stretching intensity of the complexes to that of H_2O. In the fundamental region, $H_2O{\cdot}H_2O$, $H_2O{\cdot}N_2$, and to a much lesser extent $H_2O{\cdot}O_2$, show increased OH-stretching intensity relative to H_2O. For the first overtone transitions, the intensity of the complexes is less than that of H_2O. In the higher overtone regions, the total OH-stretching intensities for $H_2O{\cdot}N_2$ and $H_2O{\cdot}O_2$ are slightly larger than those of H_2O and for $H_2O{\cdot}H_2O$ the total intensity approaches roughly twice that of H_2O as v increases.[10] Thus on a per water unit basis the OH-stretching overtone intensities of $H_2O{\cdot}N_2$ and $H_2O{\cdot}O_2$ are similar to those of $H_2O{\cdot}H_2O$.

The calculated intensities of the pure local mode transitions of H_2O, $H_2O{\cdot}N_2$, $H_2O{\cdot}O_2$, and the hydrogen donor water unit

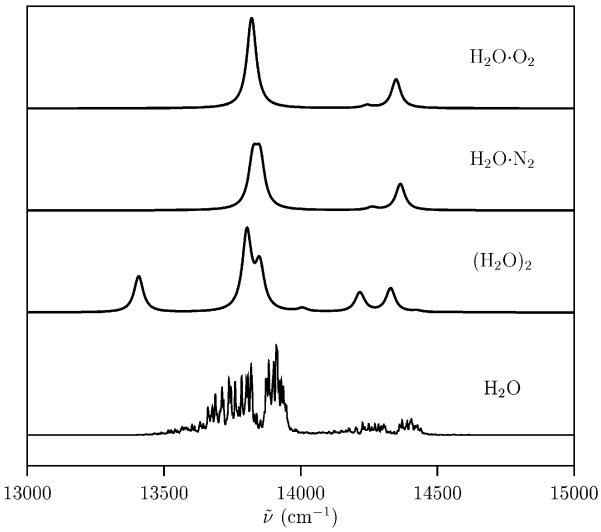

Figure 5. Simulated spectra of $H_2O{\cdot}H_2O$, $H_2O{\cdot}N_2$, and $H_2O{\cdot}O_2$ in the $\Delta v_{OH} = 4$ region. The vibrational transitions were calculated with the QCISD/6-311++G(2d,2p) method, and convoluted with Lorentzian functions with a fwhm of 40 cm^{-1}. The experimental water spectrum is taken from ref 19, where the transitions have been convoluted with Gaussian functions with a fwhm of 2 cm^{-1}.

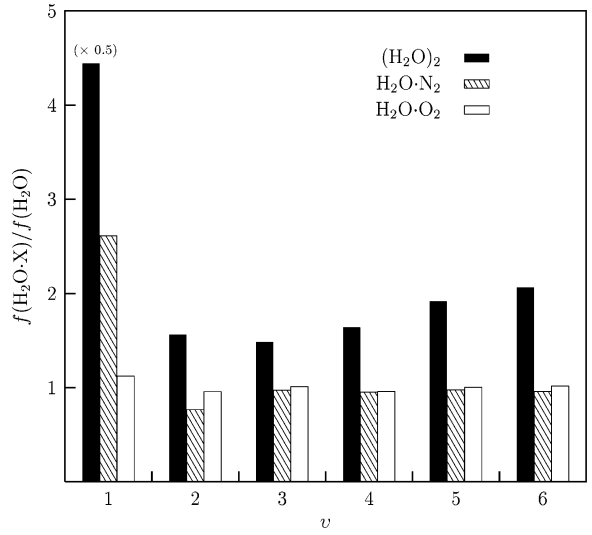

Figure 6. Ratio of total OH-stretching oscillator strength calculated for $H_2O{\cdot}H_2O$, $H_2O{\cdot}N_2$, and $H_2O{\cdot}O_2$ to that calculated for H_2O, as a function of vibrational manifold. All oscillator strengths were calculated with the QCISD/6-311++G(2d,2p) method. The intensity for $H_2O{\cdot}H_2O$ at $v = 1$ is shown at half its correct size for the purposes of clarity.

of $H_2O{\cdot}H_2O$ are shown in Table 6. The hydrogen donor water unit of $H_2O{\cdot}H_2O$ is asymmetric and the eigenstates are $|v\rangle_b|0\rangle_f$ or $|0\rangle_b|v\rangle_f$. In H_2O the two OH bonds are equivalent and the pure local mode eigenstates are symmetrized $|v0\rangle_\pm$ with the asymmetric transitions being more intense. The OH_b and OH_f bonds of $H_2O{\cdot}N_2$ and $H_2O{\cdot}O_2$ are almost equivalent and the eigenstates of the fundamental and lower overtones are significantly mixed. As v increases, the mixing becomes less and the eigenstates tend toward pure free or bonded OH-stretching states. The eigenstates of $H_2O{\cdot}N_2$ with $v \leq 2$ mix significantly and the notation in the right-hand column of Table 6 is most suitable, whereas for states with $v > 2$ the notation in the left-hand column is more applicable. For $H_2O{\cdot}O_2$ the departure from mixed states occurs at $v = 3$. It is therefore not surprising that the fundamental and first overtone OH-stretching intensities of $H_2O{\cdot}N_2$ and $H_2O{\cdot}O_2$ display behavior that is more consistent with the symmetric/asymmetric pattern of H_2O than the free/bonded pattern of the hydrogen donor unit in $H_2O{\cdot}H_2O$.

It is clear from Table 6 that the intensities of the OH-stretching transitions in $H_2O{\cdot}O_2$ are similar to those in H_2O, apart from a different splitting at higher overtones, indicating a weakly bound complex. The increase in intensity of the fundamental transitions in $H_2O{\cdot}N_2$ compared to H_2O suggests that weak hydrogen bonding is taking place. We also notice a weakening of the first overtone transitions in $H_2O{\cdot}N_2$. Both of these effects are much more pronounced in the more strongly bound $H_2O{\cdot}H_2O$ and in agreement with earlier observations for hydrogen-bonded systems.[36,37,55]

Previously, intensity changes on hydrogen bonding have been discussed in a perturbed harmonic oscillator basis.[39,56] However, the anharmonic oscillator local mode model is more suitable to describe OH_b-stretching fundamental and overtone intensities. The intensity of a one-dimensional (1D) OH_b-stretching oscillator depends on the transition dipole matrix element of eq 1, which for a 1D dipole moment function expansion similar to eq 7 can be written as

$$\langle v|\vec{\mu}|0\rangle = \vec{\mu}_1\langle v|q|0\rangle + \vec{\mu}_2\langle v|q^2|0\rangle + ... \qquad (9)$$

and the intensity changes are explained simply from the Morse oscillator matrix elements and dipole moment expansion coefficients of the OH_b-stretching oscillator. The matrix elements $\langle v|q^n|0\rangle$ calculated for a typical OH-stretching oscillator are given in Table 7. Little variation in $\langle v|q^n|0\rangle$ is found for the various OH oscillators compared here. It is obvious from the elements in Table 7 that the fundamental ($v = 1$) intensity is predominantly determined by the $n = 1$ term, which is about 20 times larger than the $n = 2$ term. This explains why fundamental intensities are usually successfully calculated with the HOLD approximations used in programs such as Gaussian.[48] For the first overtone ($v = 2$), we see that the $n = 1$ and $n = 2$ terms are of similar size and have opposite signs. Thus both terms are likely to contribute significantly to the intensity. For the higher overtones ($v = 3-5$) the absolute magnitude of the $n = 2$ term is the largest.

The ab initio calculated expansion coefficients $\vec{\mu}_i$ of the OH_b bond are given in Table 8. The smaller $\vec{\mu}_i^x$ components have been left out. It is evident from Table 8 that the sizes of $\vec{\mu}_1$ and $\vec{\mu}_2$ increase with increasing hydrogen bond strength from H_2O to $H_2O{\cdot}N_2$ to $H_2O{\cdot}H_2O$. The increase in $\vec{\mu}_1$ explains the increased fundamental intensity in $H_2O{\cdot}N_2$ and $H_2O{\cdot}H_2O$. For these two complexes, $\vec{\mu}_1$ and $\vec{\mu}_2$ have the same sign, and for the first overtone, this will lead to a cancellation of the intensity contributions as the matrix elements have opposite signs (Table 7). For $H_2O{\cdot}H_2O$ the cancellation is almost perfect and the calculated intensity of the transition to $|0\rangle_f|2\rangle_b$ is very low,[10] in good agreement with the lack of observation of the first OH_b-stretching overtone in the recent matrix isolation spectra.[36,37] For the more weakly bound $H_2O{\cdot}N_2$ the sizes of $\vec{\mu}_1$ and $\vec{\mu}_2$ are somewhat different and the cancellation is not nearly as complete as for the $|0\rangle_f|2\rangle_b$ transition in $H_2O{\cdot}H_2O$. This is evident in the calculated intensities given in Table 6. The dipole expansion coefficients for $H_2O{\cdot}O_2$ are similar to those of H_2O. We suggest that the magnitude and sign of the $\vec{\mu}_1$ and $\vec{\mu}_2$ coefficients are sensitive indicators of the strength of the hydrogen bond.

It has recently been shown that $H_2O{\cdot}H_2O$ contributes a nonnegligible amount to the atmospheric absorption of solar radiation.[42] A significant fraction of this absorption arises from the transitions that have frequencies close to the center of the water monomer transitions.[42] The dominant OH-stretching overtone transitions in $H_2O{\cdot}O_2$ and $H_2O{\cdot}N_2$ are of intensity

TABLE 6: Calculated Intensities of Pure Local Mode OH-Stretching Transitions in $H_2O\cdot N_2$, $H_2O\cdot O_2$, the Hydrogen Donor Water Unit of $H_2O\cdot H_2O$, and H_2O[a]

eigenstate[b]	$H_2O\cdot H_2O$	$H_2O\cdot N_2$	$H_2O\cdot O_2$	H_2O	eigenstate[c]
$\|1\rangle_b\|0\rangle_f$	4.86×10^{-5}	1.87×10^{-5}	0.94×10^{-5}	0.79×10^{-5}	$\|10\rangle_-$
$\|0\rangle_b\|1\rangle_f$	1.70×10^{-5}	0.48×10^{-5}	0.07×10^{-5}	0.11×10^{-5}	$\|10\rangle_+$
$\|2\rangle_b\|0\rangle_f$	0.02×10^{-8}	4.52×10^{-7}	6.27×10^{-7}	6.28×10^{-7}	$\|20\rangle_-$
$\|0\rangle_b\|2\rangle_f$	3.82×10^{-7}	1.19×10^{-7}	0.94×10^{-7}	1.24×10^{-7}	$\|20\rangle_+$
$\|3\rangle_b\|0\rangle_f$	0.18×10^{-8}	1.41×10^{-8}	1.92×10^{-8}	1.99×10^{-8}	$\|30\rangle_-$
$\|0\rangle_b\|3\rangle_f$	1.02×10^{-8}	0.60×10^{-8}	0.15×10^{-8}	0.11×10^{-8}	$\|30\rangle_+$
$\|4\rangle_b\|0\rangle_f$	3.44×10^{-10}	4.42×10^{-10}	5.56×10^{-10}	8.33×10^{-10}	$\|40\rangle_-$
$\|0\rangle_b\|4\rangle_f$	4.32×10^{-10}	4.41×10^{-10}	3.15×10^{-10}	0.20×10^{-10}	$\|40\rangle_+$
$\|5\rangle_b\|0\rangle_f$	4.86×10^{-11}	3.45×10^{-11}	3.99×10^{-11}	6.05×10^{-11}	$\|50\rangle_-$
$\|0\rangle_b\|5\rangle_f$	2.98×10^{-11}	3.96×10^{-11}	3.52×10^{-11}	1.29×10^{-11}	$\|50\rangle_+$
$\|6\rangle_b\|0\rangle_f$	7.16×10^{-12}	4.41×10^{-12}	5.31×10^{-12}	7.71×10^{-12}	$\|60\rangle_-$
$\|0\rangle_b\|6\rangle_f$	3.44×10^{-12}	5.38×10^{-12}	4.91×10^{-12}	2.01×10^{-12}	$\|60\rangle_+$

[a] Calculated with the QCISD/6-311++G(2d,2p) method and local mode parameters from Table 1. [b] Notation suitable for the hydrogen donor unit of $H_2O\cdot H_2O$. [c] Notation suitable for H_2O.

TABLE 7: Matrix Elements $\langle v|q^n|0\rangle$ of a Typical OH-Stretching Morse Oscillator (in Å^n)[a]

v	$n=1$	$n=2$	$n=3$	$n=4$
1	6.85×10^{-2}	0.35×10^{-2}	0.11×10^{-2}	0.01×10^{-2}
2	-7.20×10^{-3}	6.19×10^{-3}	0.59×10^{-3}	0.23×10^{-3}
3	1.25×10^{-3}	-1.63×10^{-3}	0.60×10^{-3}	0.08×10^{-3}
4	-2.85×10^{-4}	4.53×10^{-4}	-2.93×10^{-4}	0.53×10^{-4}
5	0.78×10^{-4}	-1.41×10^{-4}	1.19×10^{-4}	-0.47×10^{-4}

[a] Calculated with experimental local mode parameters for the water monomer $\tilde{\omega} = 3869.9$ cm^{-1} and $\tilde{\omega}x = 82.06$ cm^{-1} from ref 18.

TABLE 8: Dipole Moment Expansion Coefficients for Selected OH-Stretching Bonds[a]

molecule	bond	$\vec{\mu}_1^z$ (D Å^{-1})	$\vec{\mu}_2^z$ (D Å^{-2})	$\vec{\mu}_3^z$ (D Å^{-3})
H_2O	OH	0.76	−0.60	−1.05
$H_2O\cdot O_2$	OH_b	0.69	−0.56	−1.03
$H_2O\cdot N_2$	OH_b	1.45	0.57	0.34
$H_2O\cdot H_2O$	OH_b	2.53	2.66	2.41

[a] Calculated with the QCISD/6-311++G(2d,2p) method. The *z*-axis is along the OH_b bond in the complexes and along the OH bond in H_2O.

comparable to those in $H_2O\cdot H_2O$ and the atmospheric abundances of $H_2O\cdot O_2$ and $H_2O\cdot N_2$ have been suggested to be larger than that of $H_2O\cdot H_2O$.[28,43] Thus it is possible that $H_2O\cdot N_2$ and $H_2O\cdot O_2$ will contribute more than $H_2O\cdot H_2O$ to the atmospheric absorption of solar radiation. We suggest that the absorption from $H_2O\cdot N_2$, $H_2O\cdot O_2$, and $H_2O\cdot H_2O$ could constitute a significant fraction of the so-called water vapor continuum absorption.[57,58]

Conclusion

We have calculated the optimized geometries and the fundamental and overtone OH-stretching frequencies and intensities for $H_2O\cdot N_2$ and $H_2O\cdot O_2$. For $H_2O\cdot N_2$ the calculated lowest energy structure has N_2 positioned along one of the OH bonds in a nearly linear hydrogen bond arrangement. The $H_2O\cdot O_2$ potential energy surface is extremely flat, and the optimized geometry depended on the ab initio method. With our best ab initio method the configuration of the $H_2O\cdot O_2$ complex is one where O_2 is not aligned along an OH bond. We observe that the geometries of the monomer units are not significantly perturbed on complexation, in agreement with previous electronic structure calculations. The calculated binding energy of $H_2O\cdot N_2$ is roughly twice that of $H_2O\cdot O_2$, and both are considerably less than that of $H_2O\cdot H_2O$.

Calculations with the QCISD/6-311++G(2d,2p) method reproduce well the few experimental spectral features available for $H_2O\cdot N_2$ and $H_2O\cdot H_2O$. We believe that the HCAO method with calculated dipole moment functions is useful for predicting the OH-stretching vibrational band positions and intensities for hydrated van der Waals complexes. We find that the B3LYP level of theory largely overestimates the red shift of the hydrogen-bonded fundamental transition in $H_2O\cdot H_2O$.

The HCAO calculated OH-stretching fundamental transitions in $H_2O\cdot N_2$ and $H_2O\cdot O_2$ resemble those of H_2O. The higher energy OH-stretching band has most of the vibrational intensity, equivalent to the asymmetric stretch in H_2O. This is in contrast to the fundamental spectrum of $H_2O\cdot H_2O$, where the low-energy band corresponding to the hydrogen-bonded OH_b transition is roughly 5 times stronger than the asymmetric stretching transition in H_2O. The total fundamental OH-stretching intensity increases from H_2O and $H_2O\cdot O_2$ to $H_2O\cdot N_2$ to $H_2O\cdot H_2O$ reflecting the increasing strength of the hydrogen bond.

The overtone absorption spectra of $H_2O\cdot N_2$ and $H_2O\cdot O_2$ are dominated by transitions to pure local modes. Within each overtone the total OH-stretching oscillator strengths of $H_2O\cdot N_2$ and $H_2O\cdot O_2$ are approximately equal to those of H_2O. However, the intensity distributions in $H_2O\cdot N_2$ and $H_2O\cdot O_2$ are different from that of H_2O at higher overtones.

The intensity weakening of the first overtone hydrogen-bonded transition observed for more strongly bound complexes such as $H_2O\cdot H_2O$ and $H_2O\cdot HNO_3$ is seen only slightly in $H_2O\cdot N_2$ and is not observed in $H_2O\cdot O_2$. We explain this behavior based on the transition dipole moment matrix elements and the calculated dipole moment expansion coefficients.

The absence of significantly red-shifted OH_b bands will make atmospheric detection of the $H_2O\cdot N_2$ and $H_2O\cdot O_2$ complexes difficult. However, compared to $H_2O\cdot H_2O$ we suggest that $H_2O\cdot N_2$ and $H_2O\cdot O_2$ could contribute more to the unassigned absorption of solar radiation.

Acknowledgment. We thank Prof. J. T. Hynes and Dr. J. S. Daniel for helpful discussions. H.G.K. is grateful to CIRES for a visiting faculty fellowship. The Marsden Fund administrated by the Royal Society of New Zealand and the University of Otago have provided funding for this research.

References and Notes

(1) Cess, R. D.; Zhang, M. H.; Minnis, P.; Corsetti, L.; Dutton, E. G.; Forgan, B. W.; Garber, D. P.; Gates, W. L.; Hack, J. J.; Harrison, E. F.; Jing, X.; Kiehl, J. T.; Long, C. N.; Morcrette, J.-J.; Potter, G. L.; Ramanathan, V.; Subasilar, B.; Whitlock, C. H.; Young, D. F.; Zhou, Y. *Science* **1995**, *267*, 496.

(2) Li, Z.; Barker, H. W.; Moreau, L. *Nature* **1995**, *376*, 486.

(3) Ramanathan, V.; Subasilar, B.; Zhang, G. J.; Conant, W.; Cess, R. D.; Kiehl, J. T.; Grassl, H.; Shi, L. *Science* **1995**, *267*, 499.

(4) Pilewskie, P.; Valero, F. P. J. *Science* **1995**, *267*, 1626.
(5) Varanasi, P.; Chou, S.; Penner, S. S. *J. Quant. Spectrosc. Radiat. Transfer* **1968**, *8*, 1537.
(6) Bohlander, R. A.; Emery, R. J.; Llewellyn-Jones, D. T.; Gimmestad, G. G.; Gebbie, H. A.; Simpson, O. A.; Gallagher, J. J.; Perkowitz, S. Excess absorption by water vapor and comparison with theoretical dimer absorption. In *Atmospheric Water Vapor*; Deepak, A., Wilkerson, T. D., Ruhnke, L. H., Eds.; Academic Press: New York, 1980.
(7) Gebbie, H. A. Observations of Anomalous Absorption in the Atmosphere. In *Atmospheric Water Vapor*; Deepak, A., Wilkerson, T. D., Ruhnke, L. H., Eds.; Academic Press: New York, 1980.
(8) Chýlek, P.; Geldart, D. J. W. *Geophys. Res. Lett.* **1997**, *24*, 2015.
(9) Vigasin, A. A. Dimeric Absorption in the Atmosphere. In *Molecular Complexes in Earth's Planetary, Cometary and Interstellar Atmospheres*; Vigasin, A. A., Slanina, Z., Eds.; World Scientific: River Edge, NJ, 1998.
(10) Low, G. R.; Kjaergaard, H. G. *J. Chem. Phys.* **1999**, *110*, 9104.
(11) Henry, B. R. *Acc. Chem. Res.* **1977**, *10*, 207.
(12) Sage, M. L.; Jortner, J. *Adv. Chem. Phys.* **1981**, *47*, 293.
(13) Mortensen, O. S.; Henry, B. R.; Mohammadi, M. A. *J. Chem. Phys.* **1981**, *75*, 4800.
(14) Tarr, A. W.; Zerbetto, F. *Chem. Phys. Lett.* **1989**, *154*, 273.
(15) Kjaergaard, H. G.; Henry, B. R. *J. Chem. Phys.* **1992**, *96*, 4841.
(16) Kjaergaard, H. G.; Yu, H.; Schattka, B. J.; Henry, B. R.; Tarr, A. W. *J. Chem. Phys.* **1990**, *93*, 6239.
(17) Kjaergaard, H. G.; Turnbull, D. M.; Henry, B. R. *J. Chem. Phys.* **1993**, *99*, 9438.
(18) Kjaergaard, H. G.; Henry, B. R.; Wei, H.; Lefebvre, S.; Carrington, T., Jr.; Mortensen, O. S.; Sage, M. L. *J. Chem. Phys.* **1994**, *100*, 6228.
(19) Rothman, L. S.; Rinsland, C. P.; Goldman, A.; Massie, S. T.; Edwards, D. P.; Flaud, J.-M.; Perrin, A.; Camy-Peyret, C.; Dana, V.; Mandin, J.-Y.; Schroeder, J.; McCann, A.; Gamache, R. R.; Wattson, R. B.; Yoshino, K.; Chance, K. V.; Jucks, K. W.; Brown, L. R.; Nemtchinov, V.; Varanasi, P. *J. Quant. Spectrosc. Radiat. Transfer* **1998**, *60*, 665.
(20) Kjaergaard, H. G.; Henry, B. R. *Mol. Phys.* **1994**, *83*, 1099.
(21) Kjaergaard, H. G.; Daub, C. D.; Henry, B. R. *Mol. Phys.* **1997**, *90*, 201.
(22) Sowa, M. G.; Henry, B. R.; Mizugai, Y. *J. Phys. Chem.* **1991**, *95*, 7659.
(23) Kjaergaard, H. G. *J. Phys. Chem. A* **2002**, *106*, 2979.
(24) Andrews, L.; Davis, S. R. *J. Chem. Phys.* **1985**, *83*, 4983.
(25) Coussan, S.; Loutellier, A.; Perchard, J. P.; Racine, S.; Bouteiller, Y. *J. Mol. Struct.* **1998**, *471*, 37.
(26) Leung, H. O.; Marshall, M. D.; Suenram, R. D.; Lovas, F. J. *J. Chem. Phys.* **1989**, *90*, 700.
(27) Cacace, F.; de Petris, G.; Pepi, F.; Troiani, A. *Angew. Chem., Int. Ed.* **2000**, *39*, 367.
(28) Svishchev, I. M.; Boyd, R. J. *J. Phys. Chem. A* **1998**, *102*, 7294.
(29) Sadlej, J.; Rowland, B.; Devlin, J. P. *J. Chem. Phys.* **1995**, *102*, 4804.
(30) Mokomela, T. D.; Rencken, I.; Yeo, G. A.; Ford, T. A. *J. Mol. Struct.* **1992**, *275*, 33.
(31) Reed, A. E.; Weinhold, F.; Curtiss, L. A.; Pochatko, D. J. *J. Chem. Phys.* **1986**, *84*, 5687.
(32) Dos Santos, D. H. V.; Vaughn, S. J.; Akhmatskaya, E. V.; Vincent, M. A.; Masters, A. J. *J. Chem. Soc., Faraday Trans.* **1997**, *93*, 2781.
(33) Palmer, I. J.; Byers Brown, W.; Hillier, I. H. *J. Chem. Phys.* **1996**, *104*, 3198.
(34) Huang, Z. S.; Miller, R. E. *J. Chem. Phys.* **1989**, *91*, 6613.
(35) Huisken, F.; Kaloudis, M.; Kulcke, A. *J. Chem. Phys.* **1996**, *104*, 17.
(36) Perchard, J. P. *Chem. Phys.* **2001**, *273*, 217.
(37) Perchard, J. P. *Chem. Phys.* **2001**, *266*, 109.
(38) *Theoretical Treatments of Hydrogen Bonding*; Hadzi, D., Ed.; John Wiley & Sons, Ltd.: Chichester, 1997.
(39) Di Paolo, T.; Bourderon, C.; Sandorfy, C. *Can. J. Chem.* **1972**, *50*, 3161.
(40) Pfeilsticker, K.; Erle, F.; Platt, U. *J. Atmos. Sci.* **1997**, *54*, 933.
(41) Solomon, S.; Portmann, R. W.; Sanders, R. W.; Daniel, J. S. *J. Geophys. Res., D: Atmos.* **1998**, *103*, 3847.
(42) Vaida, V.; Daniel, J. S.; Kjaergaard, H. G.; Goss, L. M.; Tuck, A. F. *Q. J. R. Meteor. Soc.* **2001**, *127*, 1627.
(43) Vaida, V.; Headrick, J. E. *J. Phys. Chem. A* **2000**, *104*, 5401.
(44) Atkins, P. W.; Friedman, R. S. *Molecular Quantum Mechanics*, 3rd ed.; Oxford University Press: Oxford, 1997.
(45) Messiah, A. *Quantum Mechanics*; Wiley: New York, 1961; Vol. 1.
(46) Scott, A. P.; Radom, L. *J. Phys. Chem.* **1996**, *100*, 16502.
(47) Kjaergaard, H. G.; Robinson, T. W.; Brooking, K. A. *J. Phys. Chem. A* **2000**, *104*, 11297.
(48) Frisch, M. J.; Trucks, G. W.; Schlegel, H. B.; Gill, P. M. W.; Johnson, B. G.; Robb, M. A.; Cheeseman, J. R.; Keith, T.; Petersson, G. A.; Montgomery, J. A.; Raghavachari, K.; Al-Laham, M. A.; Zakrzewski, V. G.; Ortiz, J. V.; Foresman, J. B.; Cioslowski, J.; Stefanov, B. B.; Nanayakkara, A.; Challacombe, M.; Peng, C. Y.; Ayala, P. Y.; Chen, W.; Wong, M. W.; Andres, J. L.; Replogle, E. S.; Gomperts, R.; Martin, R. L.; Fox, D. J.; Binkley, J. S.; Defrees, D. J.; Baker, J.; Stewart, J. P.; Head-Gordon, M.; Gonzalez, C.; Pople, J. A. *Gaussian94*, Revision D.4; Gaussian Inc.: Pittsburgh, PA, 1995.
(49) Byers Brown, W.; Vincent, M. A.; Trollope, K.; Hillier, I. H. *Chem. Phys. Lett.* **1992**, *192*, 213.
(50) van Duijneveldt-van de Rijdt, J. G. C. M.; van Duijneveldt, F. B. Ab Initio Methods Applied to Hydrogen-bonded Systems. In *Theoretical Treatments of Hydrogen Bonding*; Hadzi, D., Ed.; Wiley: New York, 1997.
(51) Curtiss, L. A.; Melendres, C. A. *J. Phys. Chem.* **1984**, *88*, 1325.
(52) Fellers, R. S.; Leforestier, C.; Braly, L. B.; Brown, M. G.; Saykally, R. J. *Science* **1999**, *284*, 945.
(53) Curtiss, L. A.; Frurip, D. J.; Blander, M. *J. Chem. Phys.* **1979**, *71*, 2703.
(54) Guo, H.; Sirois, S.; Proynov, E. I.; Salahub, D. R. Density Functional Theory and its Applications to Hydrogen-bonded Systems. In *Theoretical Treatments of Hydrogen Bonding*; Hadzi, D., Ed.; Wiley: New York, 1997.
(55) Bourderon, C.; Sandorfy, C. *J. Chem. Phys.* **1973**, *59*, 2527.
(56) Singh, S.; Luck, W. A. P. *Chem. Phys. Lett.* **1981**, *78*, 117.
(57) Clough, S. A.; Kneizys, F. X.; Davies, R.; Gamache, R.; Tipping, R. In *Atmospheric Water Vapor*; Deepak, A., Wilkerson, T. D., Ruhnke, L. H., Eds.; Academic Press: New York, 1980.
(58) Clough, S. A.; Kneizys, F. X.; Davies, R. W. *Atmos. Res.* **1989**, *23*, 229.